Article

Synthesis of CuInS, CuInSe, and Cu(InGa)Se (CIGS) Nanocrystal "Inks" for Printable Photovoltaics

Matthew G. Panthani, Vahid Akhavan, Brian Goodfellow, Johanna P. Schmidtke, Lawrence Dunn, Ananth Dodabalapur, Paul F. Barbara, and Brian A. Korgel

J. Am. Chem. Soc., **2008**, 130 (49), 16770-16777 • DOI: 10.1021/ja805845q • Publication Date (Web): 17 November 2008

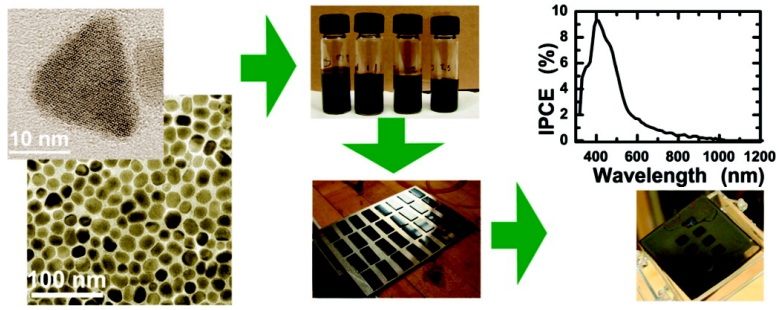

More About This Article

Additional resources and features associated with this article are available within the HTML version:

- Supporting Information
- Access to high resolution figures
- Links to articles and content related to this article
- Copyright permission to reproduce figures and/or text from this article

View the Full Text HTML

J|A|C|S
ARTICLES

Published on Web 11/17/2008

Synthesis of $CuInS_2$, $CuInSe_2$, and $Cu(In_xGa_{1-x})Se_2$ (CIGS) Nanocrystal "Inks" for Printable Photovoltaics

Matthew G. Panthani,[†] Vahid Akhavan,[†] Brian Goodfellow,[†] Johanna P. Schmidtke,[‡] Lawrence Dunn,[§,||] Ananth Dodabalapur,[§] Paul F. Barbara,[‡] and Brian A. Korgel*[,†]

Departments of Chemical Engineering, Chemistry & Biochemistry, and Physics and Microelectronics Research Center, Texas Materials Institute and Center for Nano- and Molecular Science and Technology, The University of Texas at Austin, Austin, Texas 78712-1062

Received July 25, 2008; E-mail: korgel@che.utexas.edu

Abstract: Chalcopyrite copper indium sulfide ($CuInS_2$) and copper indium gallium selenide ($Cu(In_xGa_{1-x})Se_2$; CIGS) nanocrystals ranging from ~5 to ~25 nm in diameter were synthesized by arrested precipitation in solution. The In/Ga ratio in the CIGS nanocrystals could be controlled by varying the In/Ga reactant ratio in the reaction, and the optical properties of the $CuInS_2$ and CIGS nanocrystals correspond to those of the respective bulk materials. Using methods developed to produce uniform, crack-free micrometer-thick films, $CuInSe_2$ nanocrystals were tested in prototype photovoltaic devices. As a proof-of-concept, the nanocrystal-based devices exhibited a reproducible photovoltaic response.

Introduction

I−III−VI_2 chalcopyrite compounds, particularly copper indium gallium selenide ($Cu(In_xGa_{1-x})Se_2$; CIGS), are effective light-absorbing materials in thin-film solar cells.[1] These materials possess advantageous properties for solar applications: their band gap energy is at the red edge of the solar spectrum; they are direct band-gap semiconductors with correspondingly high optical absorption coefficients;[2,3] and CIGS materials, in contrast to other candidate materials for thin-film solar cells such as CdTe and amorphous silicon (a-Si), are stable under long-term excitation.[4] High efficiency CIGS-based devices are typically fabricated using polycrystalline films,[5] and single-junction CIGS solar cells have demonstrated nearly 20% solar energy conversion efficiency,[6] which is significantly higher than either CdTe or a-Si based devices.[7] Furthermore, CIGS devices and manufacturing processes may have less environmental impact than those with thin film materials with large amounts of Cd and Pb, like CdTe and PbSe based solar cells, although to date the highest efficiency CIGS photovoltaic (PV) devices have nonetheless required CdS buffer layers.[8]

One of the hurdles currently impeding widespread commercialization of CIGS-based solar cells is the difficulty in achieving controlled stoichiometry over large device areas, leading to high manufacturing costs and poor device yield.[9] CIGS layers in state-of-the-art devices are deposited by a multistage coevaporation process in which alternate copper, indium, and gallium layers are deposited followed by reacting with a selenium source, Se, or H_2Se gas, in the chamber.[10,11] This process is time-consuming and the CIGS stoichiometry is difficult to control—intermetallic phases can form and the Se content can vary significantly in the films.[9,12] Large material losses on the deposition chamber walls also increase cost. For all of these reasons, alternative CIGS layer deposition strategies are desired.

One approach with the potential to produce CIGS layers with controlled stoichiometry without the need for high temperature annealing is to chemically synthesize CIGS nanocrystals with controlled stoichiometry and crystal phase and disperse them in solvents, creating a paint or ink. Such an approach—of printable CIGS inks—makes accessible a range of solution-based processing techniques and may lead to inexpensive fabrication

[†] Department of Chemical Engineering.
[‡] Department of Chemistry & Biochemistry.
[§] Microelectronics Research Center.
[||] Department of Physics.

(1) Miller, A.; Mackinnon, A.; Weaire, D. *Solid State Physics* **1981**, *36*, 119–175.
(2) Devaney, W. E.; Chen, W. S.; Stewart, J. M.; Mickelsen, R. A. *IEEE Trans. Electron Devices* **1990**, *37*, 428–433.
(3) Scheer, R.; Walter, T.; Schock, H. W.; Fearheiley, M. L.; Lewerenz, H. J. *Appl. Phys. Lett.* **1993**, *63*, 3294–3296.
(4) Guillemoles, J.-F.; Kronik, L.; Cahen, D.; Rau, U.; Jasenek, A.; Schock, H.-W. *J. Phys. Chem. B* **2000**, *104*, 4849–4862.
(5) Rockett, A.; Birkmire, R. W. *J. App. Phys.* **1991**, *70*, R81–R97.
(6) Contreras, Miguel, A.; AbuShama, K. R., J.; Hasoon, F.; Young, D. L.; Egaas, B.; Noufi, R. *Prog. Photovoltaics Res. Appl.* **2005**, *13*, 209–216.
(7) Green, M. A.; Emery, K.; King, D. L.; Hishikawa, Y.; Warta, W. *Prog. Photovoltaics Res. Appl.* **2007**, *15*, 35–40.
(8) Eberspacher, C.; Fthenakis, V. M.; Moskowitz, P. D. 25th IEEE Photovoltaic Specialist Conference, IEEE: Washington, DC, 1996; pp 1417−1420.
(9) Powalla, M.; Dimmler, B. *Thin Solid Films* **2000**, *361−362*, 540–546.
(10) Repins, I.; Contreras, M. A.; Egaas, B.; DeHart, C.; Scharf, J.; Perkins, C. L.; To, B.; Noufi, R. *Prog. Photovoltaics Res. Appl.* **2008**, *16*, 235–239.
(11) Contreras, M. A.; Egaas, B.; Ramanathan, K.; Hiltner, J.; Swartzlander, A.; Hasoon, F.; Noufi, R. *Prog. Photovoltaics Res. Appl.* **1999**, *7*, 311–316.
(12) Schock, H.-W.; Noufi, R. *Prog. Photovoltaics Res. Appl.* **2000**, *8*, 151–160.

10.1021/ja805845q CCC: $40.75

routes for CIGS light-absorbing layers.[13] A chemical, solution-based approach alleviates the need for a high temperature annealing step under selenium atmosphere and may solve the CIGS "selenium problem"—that is, avoiding Se loss and achieving the correct CIGS stoichiometry in films covering large substrate areas.[14] Photovoltaic devices incorporating nanocrystalline-based CdSe/CdTe[15] and CuS[16] absorber layers have been reported and demonstrated solar energy conversion efficiencies as high as 2.9%, although a high temperature anneal at 400 °C was required. Semiconductor nanocrystals have also been combined with polymers to produce solution-processed photovoltaics, such as hybrid CdSe nanocrystal/poly-3(hexylthiophene) solar cells, which yield reported efficiencies of up to 1.7%.[17] Many different semiconductor nanocrystals can be synthesized by colloidal routes, including groups II−VI,[18] III−V,[19] I−VI.[20−22] IV−VI,[23] and IV[24−26] semiconductors, but the synthesis of I−III−VI_2 nanocrystals is much less developed. Nonetheless, there are literature reports of the synthesis of ternary chalcopyrite compound nanocrystals, such as $CuInS_2$, $CuInSe_2$, and other I−II−VI_2 semiconductor nanocrystals such as $AgInS_2$.[27−32] These nanocrystals, however, generally suffer from relatively low yields, poor crystallinity,[33] and poor uniformity in composition and phase.[3,34] This is not surprising considering that many of these systems have very complicated phase diagrams and nanocrystals can further exhibit greater phase complexity than the corresponding bulk materials.[22]

Here, we report the high-yield synthesis in solution of phase-pure nanocrystals of chalcopyrite $CuInS_2$, $CuInSe_2$, and $Cu(In_x$-$Ga_{1-x})Se_2$ with controlled In/Ga ratio. The nanocrystals disperse readily in various nonpolar solvents and can be deposited as uniform, crack-free micrometer-thick films onto glass and metal substrates. Prototype photovoltaic devices (PVs) were fabricated using $CuInSe_2$ nanocrystals as the absorber layer and exhibited a robust and reproducible photovoltaic response. The reported baseline performance (solar energy power conversion efficiencies of ∼0.2%) requires improvement, which might be achieved by additional processing steps including ligand exchange, chemical treatment, or high temperature annealing.

Experimental Details

Materials. All chemicals were used as received without further purification. Oleylamine (OLA; >70%) was obtained from Fluka; copper(II) acetylacetonate ($Cu(acac)_2$; 99.99+%), copper(I) chloride (CuCl; 99.995+%), indium(III) chloride ($InCl_3$; anyhydrous 99.99%), indium(III) acetylacetonate ($In(acac)_3$; 99.99+%), elemental sulfur (99.98%), and *o*-dichlorobenzene (DCB; 99%) from Aldrich Chemical Co.; elemental selenium (99.99%) and gallium(III) chloride ($GaCl_3$; 99.9999%) from Strem Chemicals; and chloroform (99.99%), ethanol (absolute), and tetrachloroethylene (TCE; spectrophotometric grade 99+%) from Fisher Scientific. N_2 and forming gas (7% H_2, 93%N_2) were received from Matheson Tri-Gas. Copper(I) chloride, indium(III) chloride, and gallium(III) chloride were stored in a nitrogen-filled glovebox to prevent degradation.

$CuInS_2$ Nanocrystal Synthesis. A 0.26 g (1 mmol) portion of $Cu(acac)_2$ and 0.41 g (1 mmol) of $In(acac)_3$ are added to 7 mL of DCB in a 25 mL three-neck flask in air. In a separate 25-mL three-neck flask, 0.064 g (2 mmol) of elemental sulfur is dissolved in 3 mL of DCB in air. Both flasks are then attached to a Schlenk line and purged of oxygen and water by pulling vacuum at room temperature for 30 min, followed by N_2 bubbling at 60 °C for 30 min. Between 0.5 and 2 mL (1.5 to 6 mmol) of OLA are added to the (Cu, In)-DCB mixture and both flasks are heated to 110 °C and combined, maintaining a N_2 flow. The reaction mixture is refluxed (∼182 °C) for 1 h under N_2 flow. The reaction is allowed to cool to room temperature, and the nanocrystals are separated by adding excess ethanol. The yield of solution-stable nanocrystals after purification was ∼90%.

$CuInSe_2$ Nanocrystal Synthesis. In a nitrogen-filled glovebox, 1 mmol of CuCl (0.099 g), 1 mmol of $InCl_3$ (0.221 g), and 2 mmol of elemental Se (0.158 g) are combined in a 25-mL three-neck flask with an attached condenser and stopcock valve. The stopcock valve is closed before removing the flask from the glovebox, where it is attached to a Schlenk line and placed on a heating mantle. OLA (10 mL) stored in air is injected into the flask. The flask is purged of oxygen and water by pulling vacuum at 60 °C for 1 h, followed by N_2 bubbling at 110 °C for 1 h while stirring. The mixture is then heated to 240 °C, and the reaction proceeds for 4 h under vigorous stirring. The reaction is cooled to ∼100 °C, where ∼10 mL of chloroform is added to quench the reaction and ∼5 mL of ethanol is added to precipitate the nanocrystals. After adding the ethanol, the reaction mixture is immediately removed and placed in a centrifuge tube. Reactions carried out for less than 4 h yielded nanocrystals with a larger size distribution and more agglomeration when dispersed after purification. A significant amount of poorly capped and large (up to 200 nm diameter) nanocrystals are found in the crude reaction product, which is separated from the well-capped nanocrystals. The typical product yield of the well-dispersed $CuInSe_2$ nanocrystals was ∼15%. Arrested precipitation procedures in which OLA complexes of Cu, In, and Se were formed separately and then combined at high temperature yielded nanocrystals that were very unstable when purified and redispersed.

$Cu(In,Ga)Se_2$ Nanocrystal Synthesis. A typical reaction is carried about by adding 1 mmol of CuCl (0.099 g), 2 mmol of elemental Se (0.158 g), and 1 mmol total of $InCl_3$ (0.00 to 0.221 g) and $GaCl_3$ (0.00 to 0.111 g) to a 25-mL three-neck flask with attached condenser and stopcock valve in a nitrogen-filled glovebox. The stopcock valve is closed before removing the flask from the

(13) Eberspacher, C.; Pauls, K. L.; Serra, J. P. *Mater. Res. Soc. Symp. Proc.* **2003**, *763*, B8.27.1–B8.27.6.
(14) Kumar, A. P.; Reddy, K. V. *Thin Solid Films* **1997**, *304*, 365–370.
(15) Gur, I.; Fromer, N. A.; Geier, M. L.; Alivisatos, A. P. *Science* **2005**, *310*, 462–465.
(16) Wu, Y.; Wadia, C.; Ma, W.; Sadtler, B.; Alivisatos, A. P. *Nano Lett.* **2008**, *8*, 2551–2555.
(17) Huynh, W. U.; Dittmer, J. J.; Alivisatos, A. P. *Science* **2002**, *295*, 2425–2427.
(18) Murray, C. B.; Norris, D. J.; Bawendi, M. G. *J. Am. Chem. Soc.* **1993**, *115*, 8706–8715.
(19) Micic, O. I.; Curtis, C. J.; Jones, K. M.; Sprague, J. R.; Nozik, A. J. *J. Phys. Chem.* **1994**, *98*, 4966–4969.
(20) Motte, L.; Billoudet, F.; Pileni, M. P. *J. Phys. Chem.* **1995**, *99*, 16425–16429.
(21) Larsen, T. H.; Sigman, M.; Ghezelbash, A.; Doty, R. C.; Korgel, B. A. *J. Am. Chem. Soc.* **2003**, *125*, 5638–5639.
(22) Ghezelbash, A.; Korgel, B. A. *Langmuir* **2005**, *21*, 9451–9456.
(23) Murray, C. B.; Sun, S.; Gaschler, W.; Doyle, H.; Betley, T. A.; Kagan, C. R. *IBM J. Res. Dev.* **2001**, *45*, 47.
(24) Heath, J. R.; Shiang, J. J.; Alivisatos, A. P. *J. Chem. Phys.* **1994**, *101*, 1607–1615.
(25) Holmes, J. D.; Ziegler, K. J.; Doty, R. C.; Pell, L. E.; Johnston, K. P.; Korgel, B. A. *J. Am. Chem. Soc.* **2001**, *123*, 3743–3748.
(26) Lu, X.; Korgel, B. A.; Johnston, K. P. *Chem. Mater.* **2005**, *17*, 6479–6485.
(27) Elim, H. I.; Ji, W.; Ng, M.-T.; Vittal, J. J. *Appl. Phys. Lett.* **2007**, *90*, 033106.
(28) Castro, S. L.; Bailey, S. G.; Raffaelle, R. P.; Banger, K. K.; Hepp, A. F. *J. Phys. Chem. B* **2004**, *108*, 12429–12435.
(29) Banger, K. K.; Jin, M. H.-C.; Harris, J. D.; Fanwick, P. E.; Hepp, A. F. *Inorg. Chem.* **2003**, *42*, 7713–7715.
(30) Castro, S. L.; Bailey, S. G.; Raffaelle, R. P.; Banger, K. K.; Hepp, A. F. *Chem. Mater.* **2003**, *15*, 3142–3147.
(31) Arici, E.; Sariciftci, N. S.; Meissner, D. *Adv. Funct. Mater.* **2003**, *13*, 165–171.
(32) Czekelius, C.; Hilgendorff, M.; Spanhel, L.; Bedja, I.; Lerch, M.; Müller, G.; Bloeck, U.; Su, D.-S.; Giersig, M. *Adv. Mater.* **1999**, *11*, 643–646.
(33) Eberspacher, C.; Pauls, K.; Serra, J. 28th IEEE Photovoltaic Specialist Conference; IEEE:Anchorage, AK, 2000; pp 517−520.
(34) Choi, S.-H.; Kim, E.-G.; Hyeon, T. *J. Am. Chem. Soc.* **2006**, *128*, 2520–2521.

Table 1. Measured CIGS Nanocrystal Composition

target compound	precursor composition (atom ratio % Cu/In/Ga/Se)	composition measured by EDS[a] (atom ratio % Cu/In/Ga/Se)	composition measured by ICPMS[b] (atom ratio % Cu/In/Ga/Se)
$CuInSe_2$	25:25:50 (1:1:0:2)	29:25:0:46 (1.16:1.00:0:1.84)	25:25:0:50 (1:1:0:2)
$CuIn_{0.75}Ga_{0.25}Se_2$	25:19:6:50 (1:0.76:0.24:2)	25:18:5:52 (1:0.72:0.20:2.08)	26:15:9:50 (1.04:0.60:0.36:2.00)
$CuIn_{0.50}Ga_{0.50}Se_2$	25:13:12:50 (1:0.52:0.48:2)	27:14:12:47 (1.08:0.56:0.48:1.88)	26:13:11:50 (1.04:0.52:0.44:2.00)

[a] EDS measurements have an error of ca. ±2 atom %. [b] ICPMS measurements have an error of ±0.1 atom % for Cu, ±0.2 atom % for In, ±0.1 atom % for Ga, ±0.5 atom % for Se.

glovebox, where it is attached to a Schlenk line and placed on a heating mantle. OLA (10 mL) is injected into the flask. The flask is purged of oxygen and water by pulling vacuum at 60 °C for 1 h, followed by N_2 bubbling at 110 °C for 1 h while stirring. The mixture is then heated to 240 °C, and the reaction proceeds for 4 h under vigorous stirring. The product yield of $CuIn_xGa_{1-x}Se_2$ nanocrystals with $x < 1$ ranged from 20%−60% after purification.

Nanocrystal Purification. The nanocrystal products were purified by precipitation with excess ethanol followed by centrifugation at 8000 rpm for 10 min. After such a washing step, the supernatant contains unreacted precursor and byproducts and is discarded. The nanocrystals are in the precipitate. The nanocrystals are then redispersed in 10 mL of chloroform and centrifuged at 7000 rpm for 5 min to remove poorly capped nanocrystals and large particulates, which settle during centrifugation. The well-capped nanocrystals remain dispersed in the supernatant. The precipitate is discarded and a small amount of OLA (0.2 mL) is subsequently added to the supernatant to ensure complete surface passivation of the nanocrystals. To remove excess capping ligands and remaining impurities, the product is again precipitated using ∼5 mL of ethanol and centrifuged at 8000 rpm for 10 min, then redispersed in chloroform. This process is done three times to obtain a high-purity product. The isolated nanocrystals disperse in various nonpolar organic solvents, including hexane, toluene, decane, chloroform, and TCE.

Materials Characterization. The nanocrystals were characterized using a range of analytical techniques, including transmission electron microscopy (TEM), energy-dispersive X-ray spectroscopy (EDS), inductively coupled plasma mass spectrometry (ICP-MS), scanning electron microscopy (SEM), X-ray diffraction (XRD), and UV−vis−NIR absorbance spectroscopy.

TEM imaging was performed on nanocrystals drop-cast from chloroform, hexane, or toluene dispersions on carbon-coated 200 mesh copper or nickel TEM grids (Electron Microscopy Sciences). TEM images were acquired on either a Phillips 208 TEM with 80 kV accelerating voltage or a JEOL 2010F TEM operating at 200 keV. The JEOL 2010F TEM is equipped with an Oxford INCA EDS detector, which was used to collect EDS data. The nanocrystal composition was also measured using inductively coupled mass spectrometry (ICPMS) for nanocrystal films and powders using a GBC Optimass 8000 ICP-TOF-MS. The ICPMS samples were prepared by digesting a dried nanocrystal powder or thin film in concentrated HNO_3.

SEM images were acquired using either a LEO 1530 or Zeiss Supra 40 VP SEM operated between 1 and 10 keV. For SEM imaging, the nanocrystals were deposited by evaporation from a solvent on a Si or Mo-coated glass substrate.

XRD data was acquired using a Bruker-Nonius D8 Advance $\theta-2\theta$ Powder Diffractometer equipped with a Bruker Sol-X Si(Li) solid-state detector and a rotating stage. Cu Kα ($\lambda = 1.54$ Å) radiation was used. For XRD, the nanocrystals were evaporated from concentrated dispersions onto quartz (0001) substrates as ∼0.5 mm thick films. Diffraction data was collected by scanning for 4 to 12 h with an angle increment of 0.01° or 0.02° at a scan rate of 6°/min and a rotation speed of 15 rpm.

UV−vis−NIR absorbance spectra were obtained with a Varian Cary 500 UV−vis−NIR spectrophotometer using hexane-dispersed nanocrystals in a quartz cuvette. Film thicknesses were found using a Veeco Dektak 6 M stylus profiler.

Nanocrystal Film Deposition and Photovoltaic Device Fabrication. Thick films (∼1 μm) of nanocrystals were deposited onto 12 × 25 mm glass or Mo-coated glass substrates by dropping 150 μL of TCE dispersions with nanocrystal concentrations of 5 mg/mL. The film was fully dried by placing the substrate in a vacuum chamber at room temperature for 12 h.

Photovoltaic test structures were fabricated with a conventional sandwich-type Mo/$CuInSe_2$/CdS/ZnO/indium tin oxide (ITO) configuration. The molybdenum (Mo) backcontact was first deposited on soda lime glass (Delta Technologies, 25 × 25 × 1.1 mm^3 polished float glass) by radio frequency (rf) sputtering from a pure Mo target (99.999%, Lesker) in ultrapure Ar (99.999%, Praxair) at 5 mTorr. Radio frequency sputtering was used instead of DC sputtering because it has been reported to provide a film with a better combination of substrate adhesion and good conductivity.[35] The $CuInSe_2$ nanocrystal layer was deposited by dropcasting it from TCE dispersions and then placing the film under vacuum overnight at room temperature to dry. A CdS buffer layer was deposited from solution using a procedure and parameters outlined by McCandless and Shafarman.[36] Stock aqueous solutions of 0.015 M cadmium sulfate (Aldrich, 99.999%), 1.5 M thiourea (Fluka, 99%), and 14.28 M ammonium hydroxide (Fisher Scientific, Certified ACS) were made and used in preparation of working solutions by mixing 1.25 mL of the $CdSO_4$ solution, 2.2 mL of the $CS(NH_2)_2$ solution, and 2.8 mL of the NH_4OH solution. Substrates were placed on a hot plate for 10 min that had been preheated to 90 °C, after which ∼0.5 mL of the working solution was deposited on each substrate. The substrates were immediately covered to reduce the loss of ammonia from the solution. After 2 min the substrates were removed from the hot plate, rinsed with DI water, and laid flat to dry. The *i*-ZnO/ITO top contact was deposited by rf sputtering from pure targets of each material: ZnO (99.9%, Lesker) was deposited using 0.5% O_2 in Ar (99.95%, Praxair) and ITO (99.99% In_2O_3:SnO_2 90:10, Lesker) was deposited in Ar. The final active region of the device was 8 mm^2 (a 4 mm × 2 mm rectangle).

The electrical properties of the PV devices were characterized using a Karl Suss Probe station and an Agilent 4156C Parameter Analyzer. Detailed studies of power conversion efficiencies were done using a Keithley 2400 General Purpose Sourcemeter and a Xenon Lamp Solar Simulator (Newport) equipped with an AM1.5 filter. Incident photon conversion efficiency (IPCE) spectra were gathered using a lock-in amplifier (Stanford Research Systems,

(35) Scofield, J. H.; Duda, A.; Albin, D.; Ballard, B. L.; Predecki, P. K. *Thin Solid Films* **1995**, *260*, 26–31.
(36) McCandless, B. E.; Shafarman, W. N. Chemical Surface Deposition of Ultra-thin Semiconductors. U.S. Patent 6,537,845, March 25, 2003.

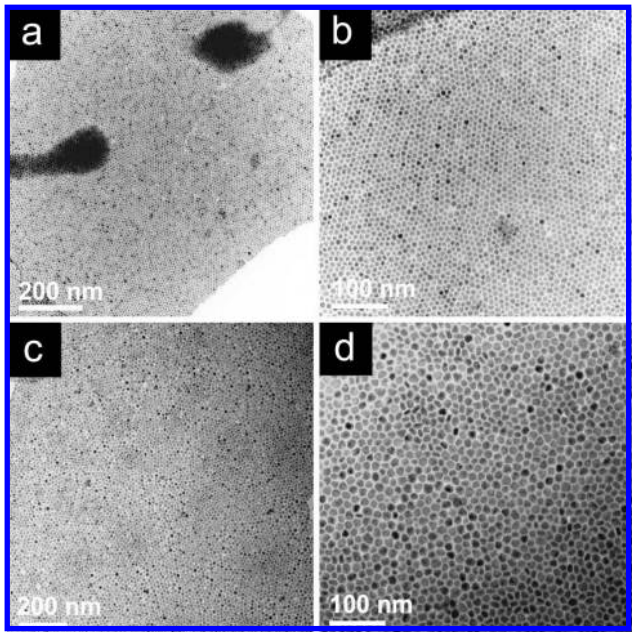

Figure 1. TEM images of $CuInS_2$ nanocrystals synthesized with varying OLA/(Cu+In) mole ratios: (a,b) 6:1, 8 nm diameter; (c,d) 3:1, 12 nm diameter.

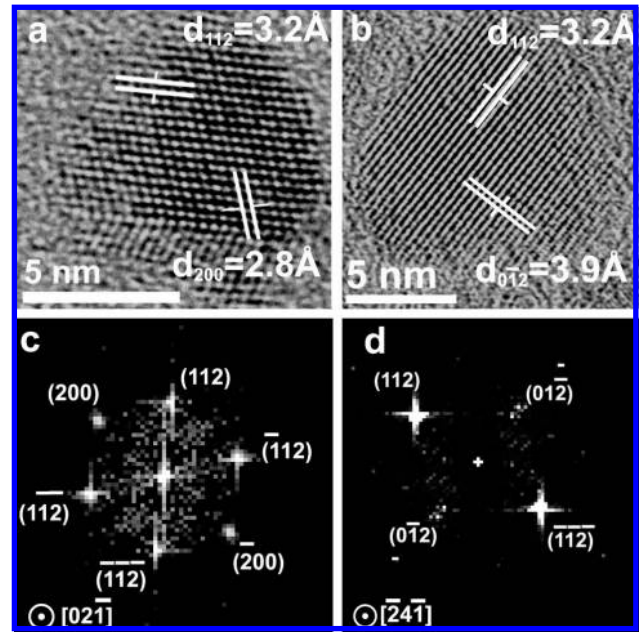

Figure 2. HRTEM images of a $CuInS_2$ Nanocrystals (a,b) and their respective fast Fourier transforms (FFTs) (c,d). The *d*-spacings correspond to chalcopyrite (tetragonal) $CuInS_2$.

model SR830), a monochromator (Newport Cornerstone 260 1/4M), and a Si photodiode calibrated by the manufacturer (Hamamatsu).

Results and Discussion

$CuInS_2$ Nanocrystals. $CuInS_2$ nanocrystals were synthesized using a variation of the procedure developed by Ghezelbash and Korgel[22] for CuS nanocrystals, by adding $In(acac)_3$ as an In source to the reaction:

$$Cu(acac)_2 + In(acac)_3 + 2S \xrightarrow[\text{oleylamine}]{\text{o-dichlorobenzene, } 180^\circ} CuInS_2 \text{ nanocrystals} + \text{byproducts} \quad (1)$$

Elemental sulfur dissolves in dichlorobenzene and could be used directly as the sulfur source. Figure 1 shows TEM images of $CuInS_2$ nanocrystals synthesized using the reaction scheme in eq 1. The nanocrystal size could be roughly controlled by varying the OLA/metal ratio. Figure 1 shows $CuInS_2$ nanocrystals with two different average diameters obtained by varying the OLA/metal ratio in the reaction. The average nanocrystal diameter was increased from 6 to 12 nm as the OLA/metal ratio by decreasing the ratio from 6:1 to 3:1. The nanocrystal shape was not perfectly spherical, which contributed to the relatively broad size distributions of the nanocrystals. High resolution TEM (Figure 2) showed the crystallinity of the nanocrystals, with lattice spacings corresponding to tetragonal $CuInS_2$. XRD (Figure 3) confirmed that the nanocrystals are chalcopyrite (tetragonal) $CuInS_2$ and that no other phases are produced in the reaction. EDS from fields of nanocrystals gave an average Cu/In/S composition of 0.29:0.25:0.46, which is near the target 0.25:0.25:0.5 ratio, considering the error of the EDS detector (approximately ±2 atom %) and that Cu is slightly overrepresented in the EDS spectra because of signal from the Cu sample holder. There was no compositional variation from particle to particle within the error of the EDS detector. The band gap energy determined from absorbance spectra (Figure 4) of optically clear (i.e., nonscattering) dispersions of nanocrystals was found to be 1.29 eV (960 nm), which is within the

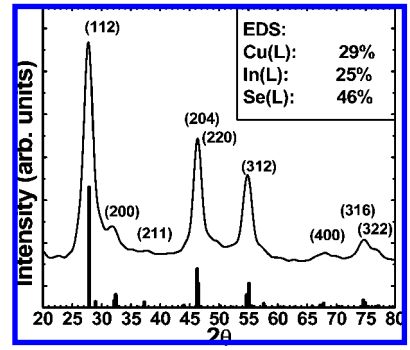

Figure 3. XRD and (inset) elemental composition measured by EDS of 8 nm diameter $CuInS_2$ nanocrystals. The peak labels correspond to those of chalcopyrite (tetragonal) $CuInS_2$ (JCPDS No. 085-1575).

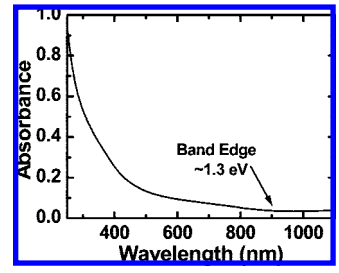

Figure 4. Room temperature absorbance spectrum of 8 nm diameter $CuInS_2$ nanocrystals dispersed in hexane.

range of the $CuInS_2$ band gap energy (which has been reported to lie between 1.2 and 1.5 eV) reported in literature.[3,37]

$CuInSe_2$ Nanocrystals. $CuInSe_2$ nanocrystals could not be synthesized using an approach similar to $CuInS_2$ because unlike S, Se does not dissolve in dichlorobenzene. After exploring a variety of different reaction approaches, one effective route was

(37) Berger, L. I. In *CRC Handbook of Chemistry and Physics*, 79 ed.; CRC Press, Boca Raton, FL, 1999; pp 12−84.

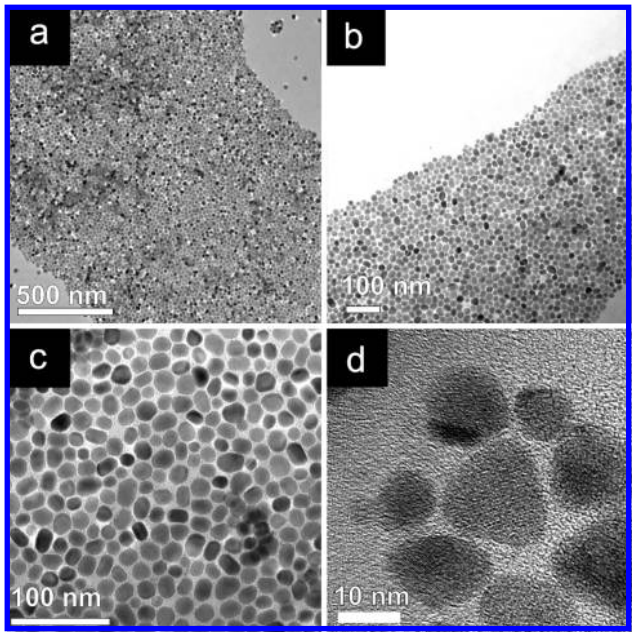

Figure 5. TEM images of $CuInSe_2$ nanocrystals with an average diameter of 15 nm.

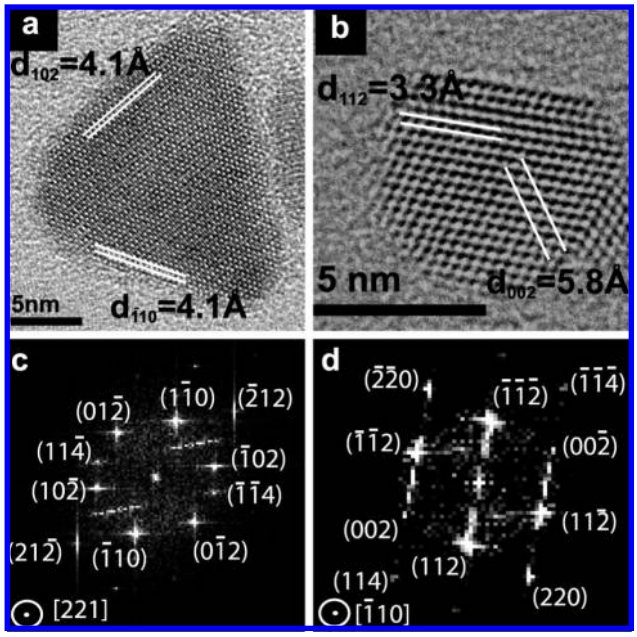

Figure 6. (a,b) HRTEM images of $CuInSe_2$ nanocrystals and (c,d) their FFTs. The observed *d*-spacings and the indexed FFTs are consistent with chalcopyrite (tetragonal) $CuInSe_2$.

a direct combination of Cu and In salts and solid Se in a flask with oleylamine followed by heating to 240 °C for 4 h:

$$CuCl + InCl_3 + 2Se \xrightarrow[240°]{\text{oleylamine}} CuInSe_2 \text{ nanocrystals} + \text{byproducts} \quad (2)$$

Figure 5 shows TEM images of a typical $CuInSe_2$ nanocrystal preparation. The nanocrystals are approximately 15 nm in diameter. Both high-resolution TEM (Figure 6) and XRD (Figure 7) confirmed that the nanocrystals are crystalline with tetragonal chalcopyrite $CuInSe_2$ structure. The *d*-spacings observed in TEM and the FFTs of the TEM images are also consistent with tetragonal $CuInSe_2$. No other crystal phases were

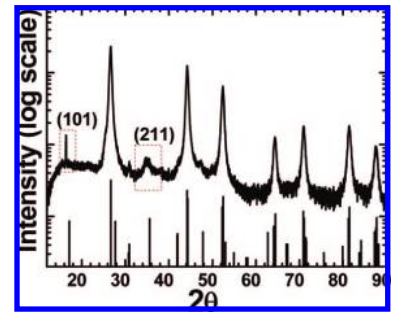

Figure 7. XRD pattern of chalcopyrite $CuInSe_2$ nanocrystals (JCPDS No. 00-040-1487). The scattering intensity is plotted on a logarithmic scale to elucidate the (211) peak. Dashed boxes indicate reflections that are unique to chalcopyrite ($CuInSe_2$).

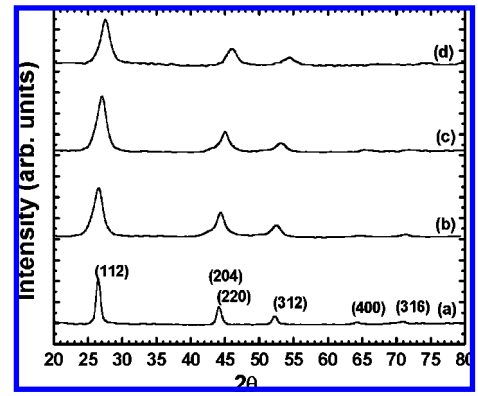

Figure 8. XRD patterns of CIGS nanocrystals synthesized with varying In:Ga ratios: (a) $CuInSe_2$ (b) $CuIn_{0.79}Ga_{0.21}Se_2$ (by EDS) (c) $CuIn_{0.51}Ga_{0.49}Se_2$ (by EDS) (d) $CuGaSe_2$ nanocrystals. The diffraction patterns correspond to those of the tetragonal chalcopyrite phases of the respective compounds. The indexing of the peaks noted in (a) correspond to the expected peaks positions of the chalcopyrite compounds.

observed in the XRD patterns of the product. Compositional analysis by ICPMS showed that the average composition of the nanocrystals in the sample has a molar Cu/In/Se ratio of 1:1:2 and the composition of individual particles measured by EDS was 1:1:2 with a variation from particle to particle less than the experimental error of ca. ±2 atom %.

Like the $CuInS_2$ nanocrystals, the $CuInSe_2$ nanocrystals are not spherical and exhibit significant faceting. The faceting has thus far been difficult to control, but this might be addressed by the optimization of several factors, including the capping-ligand chemistry and the way reactants are added to the reaction. The relatively broad size distribution of the nanocrystals (ranging from as small as 5 nm to as large as 25 nm) is largely the result of this irregularity in particle shape.

$Cu(In_x,Ga_{1-x})Se_2$ (CIGS) Nanocrystals. CIGS nanocrystals were synthesized following the approach developed for $CuInSe_2$ nanocrystals, but with the addition of $GaCl_3$ to the reaction mixture in the desired In/Ga mole ratio:

$$CuCl + xInCl_3 + (1-x)GaCl_3 + 2Se \xrightarrow[240°]{\text{oleylamine}} Cu(In_xGa_{1-x})Se_2 \text{ nanocrystals} + \text{byproducts} \quad (3)$$

The In/Ga ratio could be tuned across the entire stoichiometric range with *x* from 0 to 1 using this approach. Figure 10 shows TEM images of $CuIn_xGa_{1-x}Se_2$ with *x* ranging from 0.79 to 0. Figures 8 and 9 show XRD data of CIGS nanocrystals synthesized with Ga/In ratios varying from 0 to 1. All of the

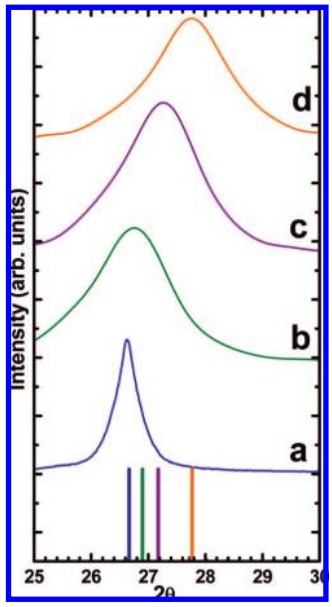

Figure 9. Magnification of the (112) XRD peaks from Figure 8 of the CIGS nanocrystals: (a) $CuInSe_2$ (b) $CuIn_{0.79}Ga_{0.21}Se_2$ (by EDS) (c) $CuIn_{0.51}Ga_{0.49}Se_2$ (by EDS) (d) $CuGaSe_2$ nanocrystals. The reference positions are for $CuInSe_2$ (JCPDS#00−040−1487), $CuIn_{07}Ga_{0.3}Se_2$ (JCPDS#00−035−1102), $CuIn_{0.5}Ga_{0.5}Se_2$ (JCPDS#00−040−1488), and $CuGaSe_2$ (JCPDS#00−031−0456).

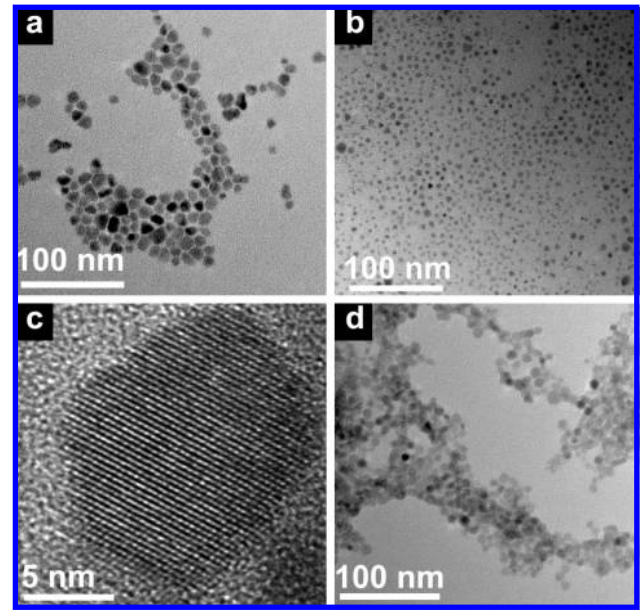

Figure 10. TEM images of $CuIn_xGa_{1-x}Se_2$ nanocrystals with (a) $x = 0.79$, (b) 0.56, (c) 0.21, and (d) 0.

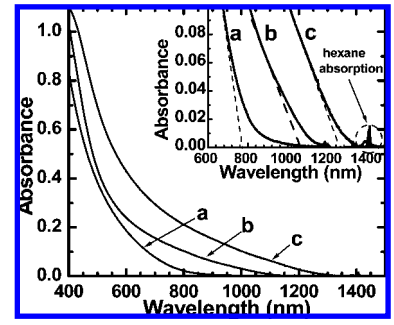

Figure 11. Room temperature absorbance spectra of $Cu(In_xGa_{1-x})Se_2$ nanocrystals dispersed in hexane. The curves correspond to In/Ga stoichiometries of (a) $x = 0$, (b) $x = 0.56$, and (c) $x = 1$. An extrapolation of the spectra to identify the band edge is shown in the inset. The small feature at ~1400 nm is related to the absorbance of hexane.

patterns are consistent with chalcopyrite (tetragonal) crystal structure and exhibit the expected amount of peak broadening due to their nanoscale crystal domain size. The diffraction peaks shift to higher 2θ with increasing Ga content, due to the decreased lattice spacing with smaller Ga atoms substituting for larger In atoms. The In/Ga ratio of the nanocrystals determined by ICPMS and EDS were consistent with the In/Ga mole ratio in the reaction mixture (see Supporting Information for sample EDS data). Additionally, EDS measurements on different nanocrystals on the substrate did not show any noticeable variation in Cu/In/Ga ratio from particle to particle in the sample. Table 1 summarizes the synthesis results. The band gap energies of the $Cu(In_xGa_{1-x})Se_2$ nanocrystals determined from room temperature absorbance spectra (Figure 11) ($CuInSe_2$, 0.95 eV; $CuIn_{0.56}Ga_{0.44}Se_2$, 1.14 eV; $CuGaSe_2$, 1.51 eV) of nanocrystal dispersions were also consistent with energies of the corresponding bulk compounds: 0.95, 1.23, and 1.6 eV.[40] The only noticeable difference in the nanocrystals with varying In/Ga ratio was that nanocrystals with higher Ga content were more difficult to stabilize in solution without aggregation. Particularly the $CuGaSe_2$ nanocrystals were not easily dispersible after isolation from the reaction mixture. More effective capping approaches to Ga-rich nanocrystals are desirable.

Deposition and Photovoltaic Response of $CuInSe_2$ Nanocrystal Layers. As a proof-of-concept, films of OLA-coated 15 nm $CuInSe_2$ nanocrystals were tested as the absorber layer in PV devices fabricated with a conventional layered Mo/$CuInSe_2$/CdS/ZnO/ITO configuration. An illustration of the device configuration is provided in the Supporting Information. Typical PV devices require relatively thick absorber layers (>1 μm), and therefore a strategy was first developed to deposit uniform, crack-free nanocrystal films.

Dip-coating worked well to deposit uniform, crack-free nanocrystal films, but only up to a maximum thickness of ~300 nm. (See Supporting Information for an example of the thickness profile of a dip-coated film.) The maximum film thickness of ~300 nm appeared to be related to the thickness of the fluid layer that formed on the vertically dipped substrate as it was pulled from the solvent. Multiple dipping steps could not improve the film thickness either as it appeared that previously deposited nanocrystals would redisperse as a new layer of particles was deposited. This fluid layer thickness depends on the substrate wettability and the dispersion viscosity and perhaps could be further improved with more study.

Uniform nanocrystal films in the appropriate thickness range could be formed by drop-casting from dispersions in high boiling point organic solvents. (See Supporting Information for SEM images of uniform, nearly crack-free films deposited from concentrated tetrachloroethylene (TCE) dispersions, along with an example of a nonuniform, heavily cracked $CuInSe_2$ nanocrystal film deposited by drop-casting from chloroform, which has a high volatility.) Nanocrystal films as thick as 3 μm could be deposited by drop-casting from concentrated TCE dispersions and the film thickness could be controlled by varying the nanocrystal concentration in the dispersions as shown in Figure 12. Figure 13 shows pictures of a TCE dispersion of $CuInSe_2$ nanocrystals and the deposition process used to make multiple films of $CuInSe_2$ nanocrystals on 12 mm × 25 mm soda-lime glass or Mo-coated glass substrates.

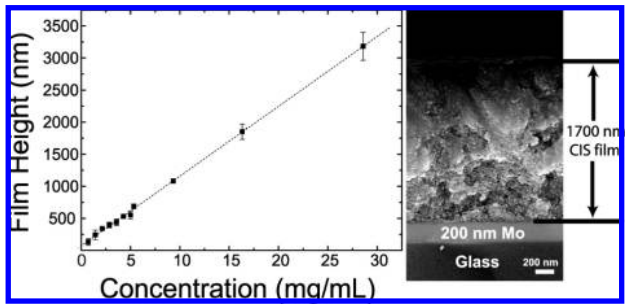

Figure 12. The thickness determined by profilometry of $CuInSe_2$ nanocrystal films drop-cast from TCE dispersions with different concentrations. The SEM image shows a cross-section of a 1.7 μm thick nanocrystal film on Mo-coated soda lime glass.

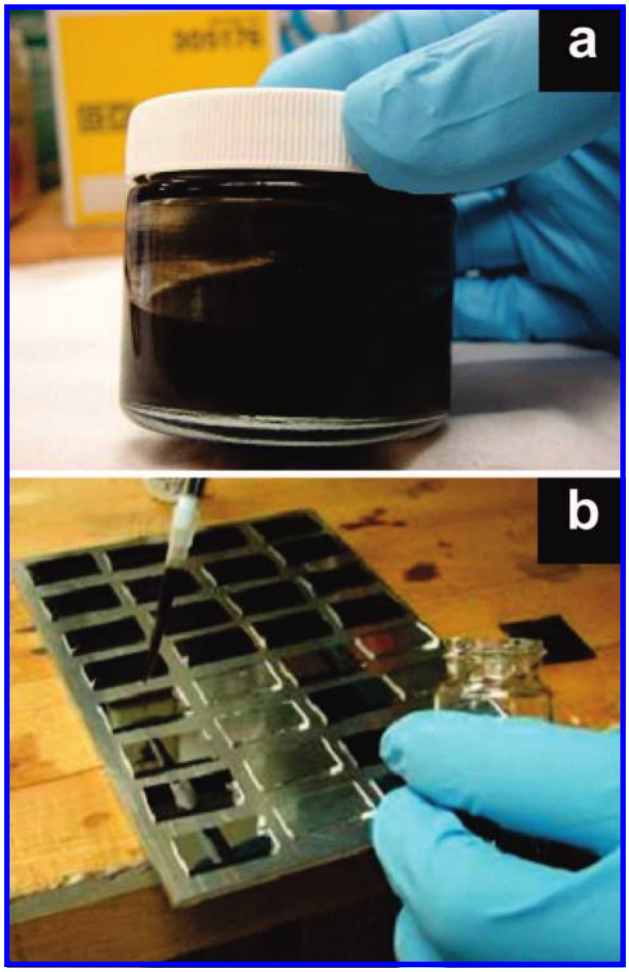

Figure 13. Photograph of (a) a $CuInSe_2$ nanocrystal dispersion and (b) the deposition of thin films on an array of glass substrates. After depositing the films, the substrates were placed in a vacuum oven at room temperature for 12 h.

The current−voltage characteristics and the incident photon conversion efficiency (IPCE) of a typical PV device made with $CuInSe_2$ nanocrystals are shown in Figure 14. The measured power conversion efficiencies (η) of 32 devices ranged between 0.01 and 0.24%. The IPCE matches approximately the absorbance spectra of the $CuInSe_2$ nanocrystals (Figure 14b), confirming that the device response results from the nanocrystals. The relatively high IPCE of ~22% for wavelengths between 400 and 500 nm tails off at higher wavelengths. The long-wavelength IPCE cutoff at ~1050 nm corresponds approximately to the optical gap of the $CuInSe_2$ nanocrystals as it should, and the sharp drop in IPCE at wavelengths <400 nm is the result of ZnO light absorption—the ZnO layer is essentially serving as a photon cutoff filter in the device.

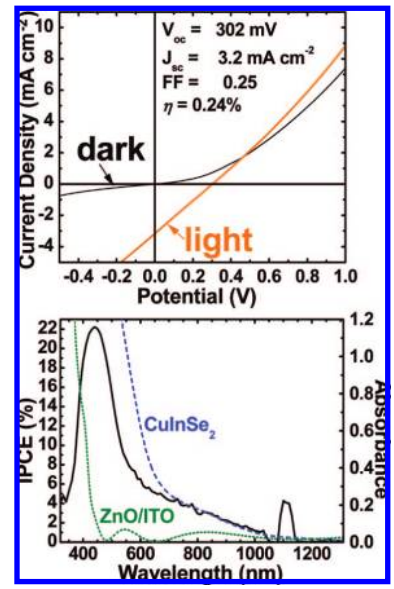

Figure 14. (a) Current−voltage characteristics and (b) IPCE spectra of a $CuInSe_2$ nanocrystal photovoltaic device (solid line) with absorbance curves of $CuInSe_2$ and ITO/ZnO layers (dashed). The IPCE spectrum was measured at zero bias. The nanocrystal absorber layer was 700 nm thick, consisting of oleylamine-capped $CuInSe_2$ nanocrystals with an average diameter of 15 nm. The measured short circuit current density in panel a corresponded to within a few percent of the integrated IPCE spectra in panel b multiplied by the AM 1.5 solar spectrum (i.e., the total number of photons converted to electrons by the device), as it should.

The photovoltaic response of devices made from $CuInSe_2$ nanocrystal layers was reproducible and demonstrated that these nanocrystals have potential as light absorbing materials in PVs. However, the PV efficiencies in these particular devices are relatively low and require significant improvement for practical applications. Device efficiencies might be improved increasing the $CuInSe_2$ film thickness to absorb more photons, and the device structures themselves are relatively complicated with many factors that can decrease efficiency. The open circuit voltages (V_{oc}) of the $CuInSe_2$ nanocrystal devices were actually quite reasonable, typically near 300 mV, which is getting close to the high-efficiency vapor-deposited $CuInSe_2$ devices (typical V_{oc} values are ~400 mV).[38] The short circuit current densities (J_{sc}) and fill factors (FF), however, were quite low, with typical J_{sc} values of ~3 mA cm^{-2} (compared to J_{sc} of ~35 mA cm^{-2} for the highest efficiency (19%) vapor-deposited CIGS device)[10] and FFs close to 0.25. The diode response was also relatively poor (see Supporting Information for data and analysis), with an ideality factor (A) much larger than 1, revealing that the device has high series and low shunt resistances.[39] The high series resistance is partly attributed to high ITO sheet resistances (>300 Ω/□) and relatively resistive nanocrystal films—four-point probe measurements gave resistivities of approximately 1 kΩ·cm, which are about 3 orders of magnitude more resistive than conventional CIGS films with good photovoltaic efficiencies.[41] High shunt conductance (or low shunt resistance) in the

(38) Stolt, L.; Hedstrom, J.; Kessler, J.; Ruckh, M.; Velthaus, K.-O.; Schock, H.-W. *Appl. Phys. Lett.* **1993**, *62*, 597–599.
(39) van Dyk, E. E.; Meyer, E. L. *Renew. Energy* **2004**, *29*, 333–344.

devices can result from many factors, including holes or cracks in the nanocrystal film and penetration of the CdS or sputtered ZnO layers to the back contact.

Conclusions

Synthetic methods for $CuInS_2$, $CuInSe_2$, and CIGS nanocrystals are described, as well as deposition approaches for achieving uniform, relatively thick ($\sim$1 μm) nanocrystal layers. Oleylamine was found to be an effective $CuInS_2$ and CIGS capping ligand. However, the stabilization of the CIGS nanocrystals with high Ga content still needs to be improved as the dispersion stability and quality of the nanocrystals decreased with increased Ga content.

Films of $CuInSe_2$ nanocrystals used as the absorber layer in conventional layered Mo/$CuInSe_2$/CdS/ZnO/ITO PV devices gave reproducible photovoltaic responses with power conversion efficiencies up to $\sim$0.2% and IPCE as high as 22% for photons with 400−500 nm wavelength. These devices provide a baseline performance and demonstrate as a proof-of-concept that these nanocrystals can be used in PVs. Practical devices, however, require higher efficiencies. There are many ways to try to improve PV efficiency, including using nanocrystals with shorter chain capping ligands, incorporating Ga into the films, and using various chemical or thermal treatments of the nanocrystal layers to increase their conductivity.[42−48] New device architectures that are more suitable to using nanocrystal absorber layers and low-temperature manufacturing steps may also provide ways to increase device efficiency and eliminate the need for high temperature processing. These are all topics for further study.

Acknowledgment. This research was supported in part by funding from the National Science Foundation through their STC program (Grant CHE-9876674), the Robert A. Welch Foundation, and the Air Force Research Laboratory (FA8650-07-2-5061).

Supporting Information Available: CIGS nanocrystal EDS data, schematic of PV device structure, thickness profile of dip-coated nanocrystal film, SEM images of drop-cast nanocrystal films, PV device diode data and analysis. This material is available free of charge via the Internet at http://pubs.acs.org.

JA805845Q

(40) Wei, S.-H.; Zhang, S. B.; Zunger, A. *Appl. Phys. Lett.* **1998**, *72*, 3199–3201.
(41) Wang, X.; Li, S. S.; Kim, W. K.; Yoon, S.; Craciun, V.; Howard, J. M.; Easwaran, S.; Manasreh, O.; Crisalle, O. D.; Anderson, T. J. *Sol. Energy Mater. Sol. Cells* **2006**, *90*, 2855–2866.
(42) Yu, D.; Wang, C.; Guyot-Sionnest, P. *Science* **2003**, *300*, 1277–1280.
(43) Talapin, D. V.; Murray, C. B. *Science* **2005**, *310*, 86–89.
(44) Urban, J. J.; Talapin, D. V.; Shevchenko, E. V.; Kagan, C. R.; Murray, C. B. *Nat. Mater.* **2007**, *6*, 115–121.
(45) Jarosz, M. V.; Porter, V. J.; Fisher, B. R.; Kastner, M. A.; Bawendi, M. G. *Phys. Rev. B* **2004**, *70*, 195327.
(46) Konstantatos, G.; Howard, I.; Fischer, A.; Hoogland, S.; Clifford, J.; Klem, E.; Levina, L.; Sargent, E. H. *Nature* **2006**, *442*, 180–183.
(47) Murphy, J. E.; Beard, M. C.; Nozik, A. J. *J. Phys. Chem. B* **2006**, *110*, 25455–25461.
(48) Law, M.; Luther, J. M.; Song, Q.; Hughes, B. K.; Perkins, C. L.; Nozik, A. J. *J. Am. Chem. Soc.* **2008**, *130*, 5974–5985.